Desalination 468 (2019) 114029

Contents lists available at ScienceDirect

Desalination

journal homepage: www.elsevier.com/locate/desal

Potential application of osmotic backwashing to brackish water desalination membranes

Asaf Dana, Sagi Hadas, Guy Z. Ramon*

Department of Civil & Environmental Engineering, Technion-Israel Institute of Technology, Haifa 32000, Israel

ARTICLE INFO

Keywords:
Reverse osmosis
Membrane fouling
Membrane cleaning
Osmotic backwashing
Direct osmosis
Desalination

ABSTRACT

Brackish water Reverse Osmosis (RO) and Nanofiltration (NF) are an attractive technology for potable water production and wastewater reclamation. However, scaling and fouling remain common problems that limit the optimal use of membranes, cause flux decline, increase energy demand and require periodic cleaning by chemical means. Herein, we consider the use of osmotic backwashing, already reported in the literature for seawater RO, as a cleaning method for brackish RO and NF. Three commercial membranes were used in a bench-scale system along with three draw solutions, NaCl, Na_2SO_4 and $MgSO_4$, to assess the osmotic flux induced during a backwash cycle. The backwash flux was found to be in good agreement with calculations made using a computational model, which was then used to reveal the role of solution chemistry as well as membrane support properties in controlling the backwash intensity and duration. Specifically, sulphate-based solutions showed a good ability to maintain an osmotic flux, better than NaCl, for which lower membrane selectivity restricts use as a draw agent. While preliminary experiments demonstrated the ability of an osmotic backwash to remove $CaPO_4$ scale, achieving nearly complete flux restoration for some cases, the process requires further optimization.

1. Introduction

The growing worldwide demand for potable water, coupled with increasing scarcity and stress on existing supplies, has prompted a tremendous technological leap in desalination, most notably Reverse Osmosis (RO) and Nanofiltration (NF). A primary reason behind the successful, large-scale deployment of these membrane-based technologies is their considerably lower energy consumption, compared with thermal evaporative techniques [1]; this is particularly so for low-salinity sources, such as wastewater. Hence, NF/RO membranes are leading candidates in wastewater reclamation for unrestricted re-use. Despite the dramatic improvement, membranes remain highly susceptible to fouling, resulting in increased operating costs [1]. In particular, the formation of scale through precipitation of sparingly-soluble salts results in a significant loss of flux through the membrane, and is considered to be the main limiting factor in the recovery ratio [2,3]. In the case of wastewater reclamation and inland brackish water desalination, this aspect is crucial, since a high recovery is necessary so that the volume of waste (the concentrated stream) is minimized.

Chemical cleaning, employed routinely at RO/NF plants, requires the shut-down of entire segments in the production, and can damage the membrane's active layer [4,5]. Advanced, in-line fouling control has been suggested in the form of an osmotic-induced backwash, which may be triggered at any time, without taking the system off-line. Osmotic backwashing, as the name implies, involves the reversal of permeation through the membrane, a concept successfully employed in microfiltration, where the flow direction is reversed by hydraulic means. In the case of thin-film composites, such hydraulic reversal is difficult in practice, as it may damage the selective ultra-thin film and require expensive, high-pressure permeate hardware. However, flow reversal may be induced when the osmotic pressure on the feed-side exceeds the applied hydraulic pressure across the membrane. This can be achieved by injection of a high osmotic pressure ‘ draw’ solution into the feed channel. Therefore, the process can have both the utility of a chemical ‘valve’, i.e. reversing or shutting off the permeation, as well as a cleaning solution with added chemical functionality, e.g. pH, detergents, chelating abilities or other.

Osmotic backwashing was first proposed by Spiegler and Macleish [6], and has since been the subject of several studies, both experimentally [7-9] as well as through theoretical models probing the characteristics of the transient osmotic flow during a backwash cycle [10-12]. To date, this method has been mostly explored in the context of Reverse Osmosis seawater desalination membranes, showing promise in the removal of organic- and bio-fouling [13,14], as well as in the context of purely osmotic processes, namely Forward Osmosis and Pressure-retarded Osmosis [15-17]. However, relatively little is known

* Corresponding author.
E-mail address: ramong@technion.ac.il (G.Z. Ramon).

https://doi.org/10.1016/j.desal.2019.05.012
Received 25 November 2018; Received in revised form 14 May 2019; Accepted 20 May 2019

on the applicability of the method for membranes intended for wastewater reclamation or brackish water desalination. In this context, Jiang et al. [18] examined the cleaning efficiency of a nanofiltration membrane from fouling during desalination of synthetic groundwater, attributed primarily to deposition of humic acid and, at shorter times, scale formed by precipitation of calcium carbonate and phosphate. They found that permeation could be fully recovered with a 10-minute backwash that is induced, after 24 h of operation, by an NaCl-based solution. These results show great promise in extending the use of osmotic backwash to low-pressure applications.

In the present study, we further explore the application of osmotic backwashing for NF and low-pressure RO membranes, experimentally and theoretically. Our primary aim is to examine membranes with different selectivity, for which the choice of osmotic agent likely impacts the ability to induce and sustain the flux reversal. A theoretical transport model is used to further explore the effect of membrane and solute parameters on the osmotic backwash. Finally, we report preliminary experiments illustrating the application of an osmotic backwash as a means for removing calcium-phosphate scale from the surface of an NF membrane.

2. Model formulation

The model employed here is a variant of the one previously used to study the dynamics of osmotic backwashing [11,13], and solves the transient advection-diffusion equation (ADE) within the membrane feed channel, which is coupled via the salt and water fluxes through the membrane, to the ADE that describes the concentration field in the support-side of the membrane. A two-dimensional (2D) computational domain is used, assuming the third dimension (the width of the membrane channel) is sufficiently large. As depicted schematically in Fig. 1 the feed (or upper) and support/permeate (or lower) domains are separated by a nonporous ultra-thin 'active' layer located at $y = 0$. The main assumption leading this model, as an extension of the previous one used in [11,13], is that the solute and solvent are transported across the active layer according to the Kedem-Katchalsky model, therefore making it applicable for non-ideal permeation, where solvent-solute coupling may not be negligible [19]. Each region in the domain has a different characteristic length, with the feed channel height and the support layer thickness denoted by δ and h_p, respectively. Here, h_p was chosen to be large enough such that the concentration profile decays far from the boundary [13].

2.1. Governing equations

In the feed and permeate space, a solute mass balance provides the ADEs [11,13]

$$\frac{\partial c_f}{\partial t} + u\frac{\partial c_f}{\partial x} + j_w\frac{\partial c_f}{\partial y} = D\left(\frac{\partial^2 c_f}{\partial x^2} + \frac{\partial^2 c_f}{\partial y^2}\right), \tag{1a}$$

$$\frac{\partial c_p}{\partial t} + j_w\frac{\partial c_p}{\partial y} = D^*\frac{\partial^2 c_p}{\partial y^2}, \tag{1b}$$

where $c_f(x,y,t)$ and $c_p(y,t)$ are the solute concentration profiles in the feed and permeate domains respectively; $u(y) = 6UY\ (1 - Y)$ is the fully developed, steady-state, axial velocity component of the feed stream with U as the maximum velocity and $Y = 2y/\delta$ is the scaled y coordinate; $j_w(x,t)$ is the water flux taken as the transverse velocity component; D^* is the modified solute molecular diffusion coefficient in the permeate space and defined as $D^* = \beta D$ where $0 < \beta \leq 1$ is the effective diffusion hindrance factor of the membrane, commonly assumed to be a simple function of the porosity, ϵ, and tortuosity, τ, of the porous support layer. In principle, the velocity component v is unknown and can be found through a solution of the Navier-Stokes equation, coupled with the mass balances (1). However, as found in previous studies [11,13] a significant computational simplification (with minor accuracy loss) may be made by assuming a fully developed, laminar velocity profile, expressed using the osmotic driven water flux. The water flux is given by,

$$j_w = -L_p(\Delta p - \sigma\Delta\pi), \tag{2}$$

where L_p is the membrane water permeability, σ is the reflection coefficient, Δp is the trans-membrane pressure difference, and $\Delta\pi$ is the trans-membrane osmotic pressure difference, given by

$$\Delta\pi = \phi i R_g T\Delta c, \tag{3}$$

where ϕ is the osmotic coefficient, i is the Van't Hoff factor, R_g is the universal gas constant, T is the absolute temperature and $\Delta c = c_{f,m} - c_{p,m}$ is the concentration difference across the 'active' layer, with subscripts f, p, m denoting the feed, permeate and membrane interface, respectively.

We now require a set of initial and boundary conditions for each side of the membrane. At the feed channel we impose

$$c_f(x, y, 0) = c_b, \tag{4a}$$

$$c_f(0, y, t) = c_b, \quad \left.\frac{\partial c_f}{\partial x}\right|_{(L,y,t)} = 0, \quad \left.\frac{\partial c_f}{\partial y}\right|_{(x,\delta,t)} = 0, \tag{4b,c,d}$$

and

$$j_w c_f(x, 0, t) - D\left.\frac{\partial c_f}{\partial y}\right|_{(x,0,t)} = j_s, \tag{4e}$$

where c_b is the bulk concentration of the draw solution and $j_s(x,t)$ is the solute flux,

$$j_s = B\Delta c - j_w(1 - \sigma)\bar{c}_m. \tag{5}$$

Here, B is the solute permeability of the membrane, j_w is again the water flux defined in Eq. (2) and $\bar{c}_m$ is the average solute concentration in the active layer. Boundary conditions (4b,c,d) represent a fixed concentration at the feed inlet, and pure advective fluxes at the upper edge and outlet of the feed space, respectively. Boundary condition (4e) is a solute mass balance on the active layer of the membrane ($y = 0$).

At the support side we impose

$$c_p(x, y, 0) = 0, \tag{6}$$

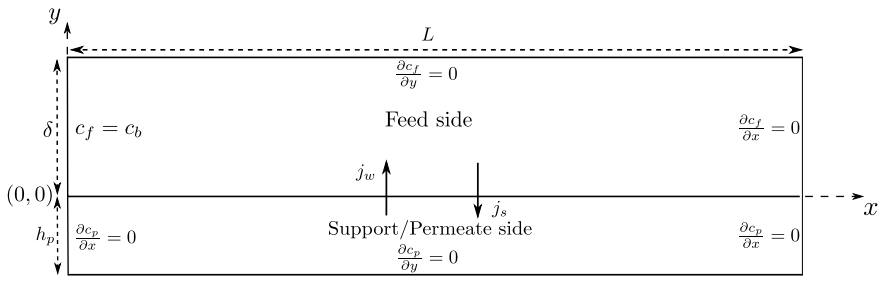

Fig. 1. A Schematic representation of the two-dimensional model coupled domain. The domain is composed of two regions, the feed channel (top) and the support layer or permeate side (bottom), separated by a nonporous ultra-thin active layer located at $y = 0$. The feed channel represents the length scale, δ, of the hydrodynamic boundary layer resulting from the cross flow of a draw-solution at the membrane edge ($y = \delta$), and the edge of the support side ($y = -h_p$) is chosen to be large enough such that the concentration gradient decays far from the boundary. The velocity field throughout the domain is represented by the axial and transverse components (u,j_w).

$$\left.\frac{\partial c_p}{\partial x}\right|_{(0,y,t)} = 0, \tag{6b}$$

$$\left.\frac{\partial c_p}{\partial x}\right|_{(L,y,t)} = 0, \tag{6c}$$

$$\left.\frac{\partial c_p}{\partial y}\right|_{(x,-h_p,t)} = 0, \tag{6d}$$

and

$$j_w c_p(x, 0, t) - D^* \left.\frac{\partial c_p}{\partial y}\right|_{(x,0,t)} = j_s, \tag{6e}$$

where j_s is again the solute flux defined in Eq. (5). The initial condition (6*a*) assumes that no solute is present in the permeate, which is incorrect since the rejection is not complete, however, the model is, in general, not very sensitive to this; (6*b*,*c*,*d*) represents the no-flux lateral boundaries of the support and the purely advective lower boundary of the support layer, respectively. Eq. (6*e*) is again the mass balance across the active layer on the support side ($y = 0$).

2.2. Computational details

The model equations were solved using the commercial finite-element package, Comsol Multyphysics v5.3a. The feed and permeate domains were meshed using a mapped variation from the membrane surface outwards, allowing for a significantly more efficient computation while retaining accuracy near the membrane surface, where the largest concentration variations were expected in the system. A time-dependent solver was employed and implemented with the 'General Form PDE' formulation, for each of the domains, fully-coupled via a flux boundary condition that was implemented using global variables for the water and salt fluxes, j_w and j_s. The parameters used in the calculations, for each of the salts and membranes used, are listed in Table 1. The diffusion coefficients used were 1.5×10^{-9}[m^2/s], 0.8×10^{-9}[m^2/s], and 0.5×10^{-9}[m^2/s] for NaCl, Na_2SO_4, and $MgSO_4$, respectively. The values of the osmotic coefficient ϕ = 0.921, 0.706, and 0.523, were obtained from the PHREEQC "Pitzer" database for NaCl, Na_2SO_4, and $MgSO_4$, respectively.

3. Experimental

Membrane characterization, fouling and cleaning experiments were performed using a bench-scale RO/NF setup composed of three high-pressure cross-flow membrane filtration cells connected in parallel. Feed solution was pumped using a diaphragm pump (Hydracell, Wanner Engineering, Minneapolis, MN, USA) controlled by a frequency converter (Schneider electric), from a stirred 20 L tank maintained at 20 ± 1°C using a circulating chiller (Thermo Fisher Scientific, USA). The membrane flow cells are made of two stainless steel plates held together by four stainless steel threaded bolts, while two O-rings provide a leak-proof seal. The dimensions of the Cross-flow channel are 60 mm (length) by 25 mm (width) and 0.8 mm (height) with a total membrane area of $1.5 \cdot 10^{-3}$ m^2. A permeate spacer is placed on the bottom plate in order to support the membrane. No feed spacers were used. A schematic illustration of the filtration system is presented in Fig. 2. The permeate collection tubes were individually drained into glass vials, with the tubes maintained filled and immersed in the vial to ensure constant permeate supply to the cells. Permeate flow rates during regular operation or backwashing, were measured by monitoring the weight of the accumulated water via 3 separate digital electronic balances, connected to a pc by a DAQ card (National Instruments) and a LabVIEW-program that acquired weight at designated time intervals; the time-rate of change in the weight was then converted to a volumetric flowrate. The tubes were connected to a bar so as to avoid their weight being supported by the collection vials. Feed conductivity was measured continuously by a conductivity probe (Thermo scientific, Eutech PC700) and permeate conductivity was measured at the end of each experiment. Experiments were repeated at least twice for each protocol with each experiment running three identical flow cells in parallel, amounting to a minimum of 6 measurement points.

Table 1
Parameters used for the computational model, Eqs. (2–6). The presented values are averages of data taken from [20-23].

	$L_p \times 10^{-12}$[m^3/m^{2}sPa]	σ[-]			$B \times 10^{-6}$[m/s]		
		NaCl	Na_2SO_4	$MgSO_4$	NaCl	Na_2SO_4	$MgSO_4$
NF90	27.2	0.83	0.98	0.97	2.54	0.14	0.092
NF270	35.2	0.24	0.99	0.96	5.64	0.25	0.24
BW30	8.26	0.98	0.98	0.98	0.92	0.0924	0.075

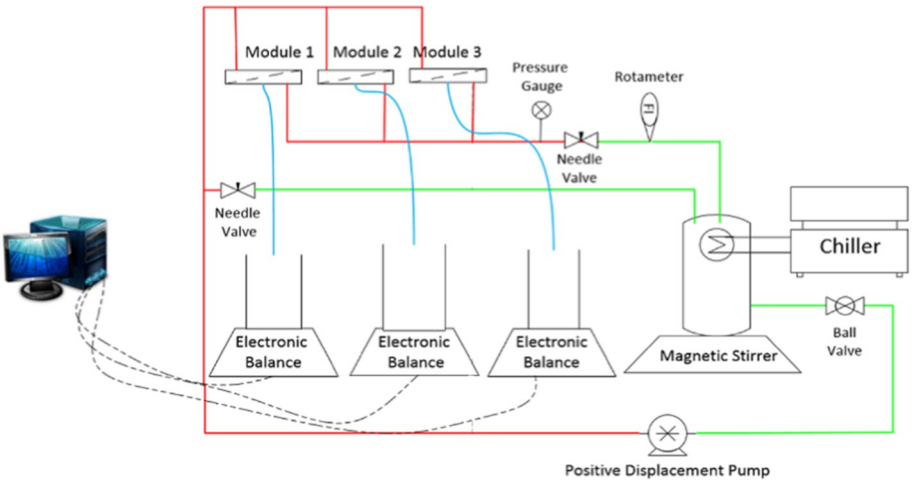

Fig. 2. Schematic drawing of the experimental system. A temperature-controlled feed tank is connected to 3 parallel-fed crossflow cells. Feed solution is delivered by a high-pressure pump with a frequency controller allowing flowrate to be varied, while the back pressure is independently regulated by a needle valve. Each permeate line is collected into beakers placed on electronic balances connected to a PC for data acquisition. During an osmotic backwash, the beakers deliver permeate back to the cells.

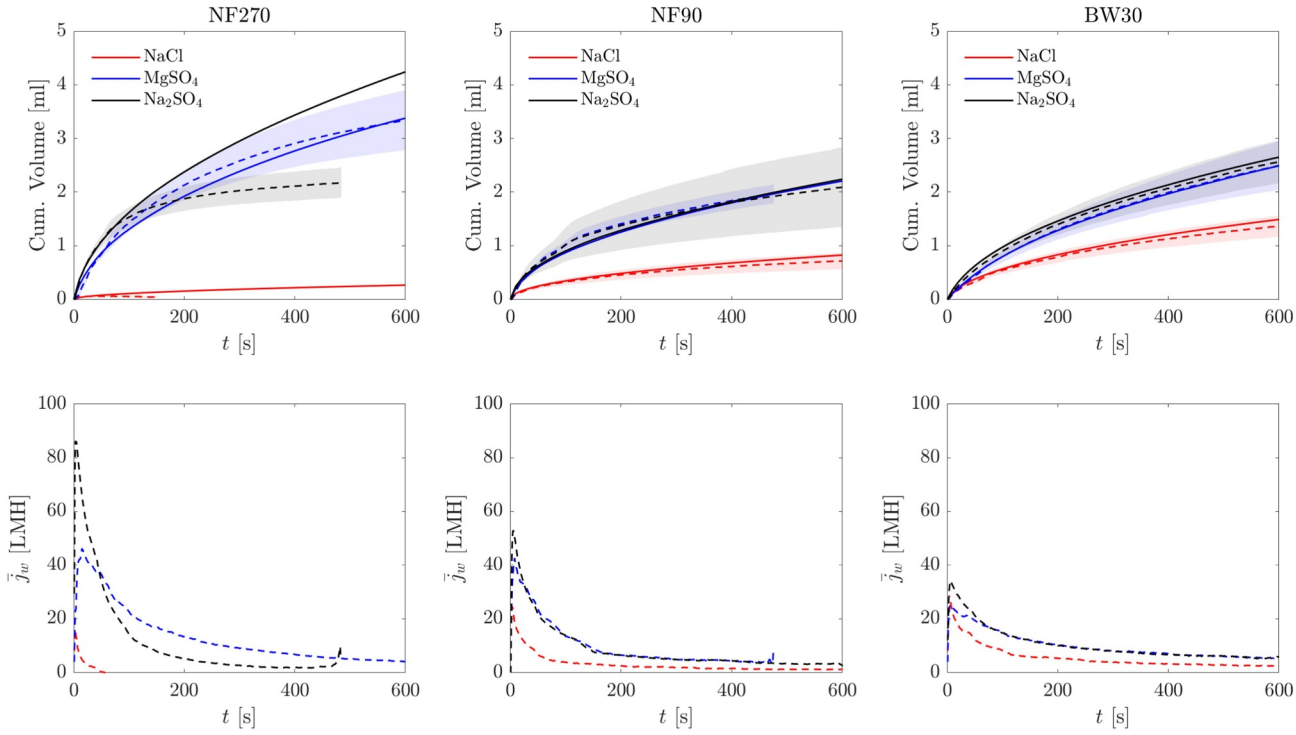

Fig. 3. The upper plots show cumulative volumes in time through three different membranes using three different salt solutions: NaCl, $MgSO_4$, and Na_2SO_4. The dashed lines are the mean experimental result, the respectively colored shades are the standard deviations and the solid lines are the numerical results of the theoretical model. The bottom plots show the calculated mean flux in Liters per m^2 per hour [LMH] vs time, obtained by the time differentiation of the mean experimental result in each respective upper plot. (a) NF270. (b) NF90. (c) BW30.

3.1. Backwash experiments

Backwash tests were conducted on 3 commercial thin-film composite membranes: NF270, NF90 and BW30 (Dow Filmtec), pre-conditioned with DI water before each of the backwashing and fouling experiments. Three different draw solutes were used - 32.56 kg/m^3 NaCl, 68.82 kg/m^3 Na_2SO_4, and 118.09 kg/m^3 $MgSO_4$; the concentration was calculated to give an osmotic pressure equal to 25 Bar according to the Van't Hoff equation (3) for non-ideal, dilute solutions, based on the PHREEQC "Pitzer" database. The crossflow flow rate was maintained at 0.5 l /min corresponding with a crossflow velocity of ~0.4 m/s or a Reynolds number of ~650 within each flow-cell.

3.2. Fouling and cleaning tests

Fouling and cleaning tests were performed on the NF90 membrane, using a 2 g /l solution of combined $CaCl_2$ and Na_2HPO_4 as the scalant. Fouling and subsequent cleaning protocols were conducted in order to test osmotic backwash (OBW) efficiency in cleaning membranes fouled by inorganic scaling. Foulant solutions were prepared by dissolving $CaCl_2$ and Na_2HPO_4 in two different glass beakers of deionized (DI) water, 4 l each, under magnetic stirring to yield a concentration of 2 [g /l] and then mixed together in the feed tank. The fouling stage was conducted at an applied pressure of 8 bar and a feed cross-flow rate identical to that of the backwash experiments (0.5 l/min for each cell, or a crossflow velocity of 0.4 m/s). Fouling was continuously monitored through the permeate flux decline. After reaching a decline greater than 50% of the initial permeate flux, the filtration process would stop, and a cleaning protocol would be initiated, consisting of reducing the applied pressure and flushing the system with either DI water, which we term 'physical washing' (PW) or by switching the feed to the osmotic draw solution (here, this was done after relieving the back-pressure valve, so backwashing proceeded without the applied pressure). The PW was conducted using DI water at zero applied pressure, with an increased cross-flow rate of 1 l/min through each cell, i.e., a crossflow velocity of ~0.8 m/s. The reversed permeate flux was measured in constant time intervals of 1 s through electronic digital scales and acquiring data via an acquisition card (DAQ) and LabVIEW software.

4. Results and discussion

4.1. Backwash flux characteristics

We begin by comparing the experimental and modeling results of the backwash tests, for the 3 membranes and 3 draw solutions. Fig. 3 shows the mean cumulative permeate volume (in dashed lines) induced through the membrane as a function of time and the standard deviations of the measurements are presented by the regions shaded in the respective colors. The experimental standard deviations were found to be in the ranges: ± 0.022, ± 0.57, ± 0.29, for NaCl, $MgSO_4$, and Na_2SO_4, respectively, with the NF270 membrane; ± 0.15, ± 0.18, ± 0.75, for NaCl, $MgSO_4$, and Na_2SO_4, respectively, with the NF90 membrane; and ± 0.19, ± 0.45, ± 0.4, for NaCl, $MgSO_4$, and Na_2SO_4, respectively, with the BW30 membrane. Solid lines show model calculations based on an estimated value of the hindrance factor β (see Table 2), which are in good agreement with the experiments, especially for solutions of divalent salts. All backwash curves exhibit similar dynamics - a distinct early-time rapid increase in accumulated volume

Table 2
Fitted values of β obtained from the numerical solutions.

	β		
	NaCl	**Na_2SO_4**	**$MgSO_4$**
NF90	0.05	0.075	0.15
NF270	0.05	0.2	0.5
BW30	0.05	0.1	0.2

(reflecting an initially high back-permeation rate), which then slowly decays in time (and conversely, a rapid decline in flux, followed by a slow decay). This behavior reflects the first stage, i.e., decay of the water flux through the membrane as a result of the decrease in concentration difference across the active layer, due to dilution of the draw solution adjacent to the membrane surface, and a slower, second stage, i.e., accumulation of salt in the support (external and internal concentration polarization, respectively). For all three membranes tested, the most rapid flux decay is observed for NaCl, compared with the sulphate-based draw solutions. This can be attributed primarily to poorer retention capability of the membranes (particularly the NF270). In general, both sulphate-based draw solutions exhibited a good ability for sustaining an osmotic flux, in all three membranes. Furthermore, we note that all cases considered have reached a significant decay in flux by approximately 600 s, suggesting that for the concentrations used, beyond this mark the backwash has no real hydrodynamic effect. However, even at this point the osmotic draw solution may still be an effective cleaning aid, as it maintains conditions of practically-zero flux, which can facilitate removal of deposited material, even under an applied pressure, since a main driver for deposition is the 'permeation drag' force [24].

4.2. Influence of process parameters on osmotic backwashing

In order to further understand the process, we use the model to explore the effect of different parameters on two main outputs: (1) the duration of an osmotic backwash, i.e., the time a given membrane can sustain an osmotic backflow; and (2) the average flux during that time, as it reflects the 'intensity' of the backwash process. To this end, we define the duration of the OBW, t_{OBW}, as the time over which the flux declines to a value of 5 μm/s ($\approx$18 LMH). Fig. 4 shows calculations of t_{OBW} for varying values of the effective hindered diffusion factor, β. An increase in β means a higher mobility of the salt inside the support layer, improving mass transfer of solute within the support. Consequently, polarization due to the water flux and salt leakage through the membrane is reduced. This improves the flux since normally polarization increases the concentration on the permeate side of the active layer causing a reduction of the driving force and, hence, the osmotic permeation rate. While NaCl is the most mobile of the draw solutes explored, it only slightly increases OBW duration in all membranes, probably due to the low rejection of the membranes towards it. Furthermore, this idea is supported by the large β behavior for BW30 (with a relatively high rejection) showing the largest OBW duration for NaCl. Better salt retention by the membrane reduces this leakage, and sustains the backwash for longer periods; in fact, under perfect retention the backwash flux would reach a steady-state value determined solely by mass transfer in the feed channel (i.e., the severity of dilutive polarization at the feed membrane interface). In conclusion, we see that membranes with lesser transport hindrance in their support and good salt retention exhibit potential for increasing the OBW duration by one or even two orders of magnitude.

The effect of the initial osmotic pressure difference across the active layer, $\Delta\pi_0$, on OBW duration is shown in Fig. 4 as the percent change relative to the value obtained for $\Delta\pi_0$ = 15bar. It is evident that NaCl benefits from this much more than the other draw solution agents, which can be explained as the result of a larger initial driving force that, therefore, takes longer to dissipate even with the relatively large leakage of NaCl. This is particularly crucial in the case of the NF270 membrane, where NaCl leakage is particularly rapid. The other combinations of membrane/draw solution mostly benefit from increased initial osmotic pressure, albeit quite moderately, likely due to the trade-off between the increased initial flux and the correspondingly rapid decline due to concentration polarization. For the case of $MgSO_4$, the backwash duration actually decreases slightly, possibly due to a lower diffusivity and hence, exacerbation of internal polarization at higher draw solution concentrations, where solute leakage is larger and, more

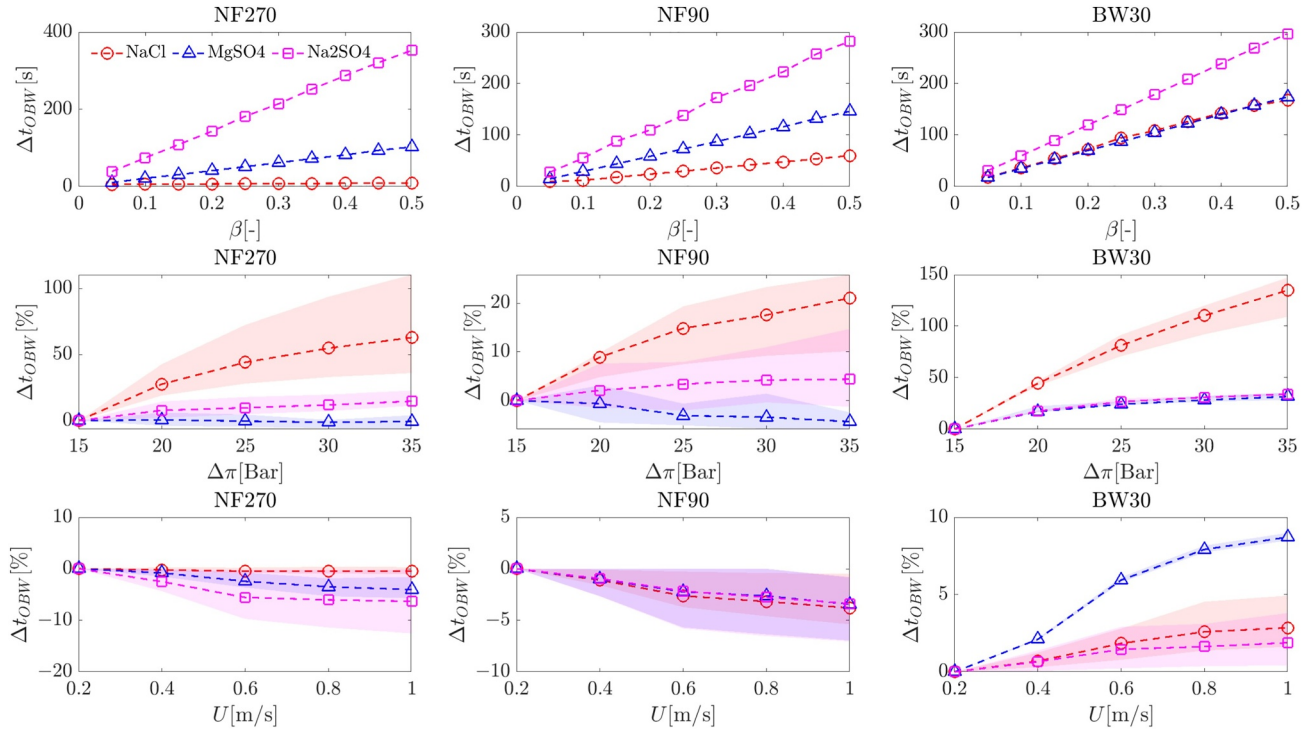

Fig. 4. Numerical solutions for the theoretical model using varying parameters and their effect on OBW duration, t_{OBW}[s], defined as the time until the water flux j_w reaches a value of 5μm/s (18 LMH). The first row shows the effect of the hindered support diffusivity β on t_{OBW}. The second and third rows show the effects due to variations in the initial osmotic pressure across the membrane $\Delta\pi$[bar] and the cross flow velocity U[m/s] in the feed side respectively. The vertical axis is the percent change in OBW duration with respect to the minimal value of the parameter (i.e. 0% change). The respectively colored shaded regions are the value ranges for different values of $\beta \in$ [0.05,0.5] and the solid lines are the mean.

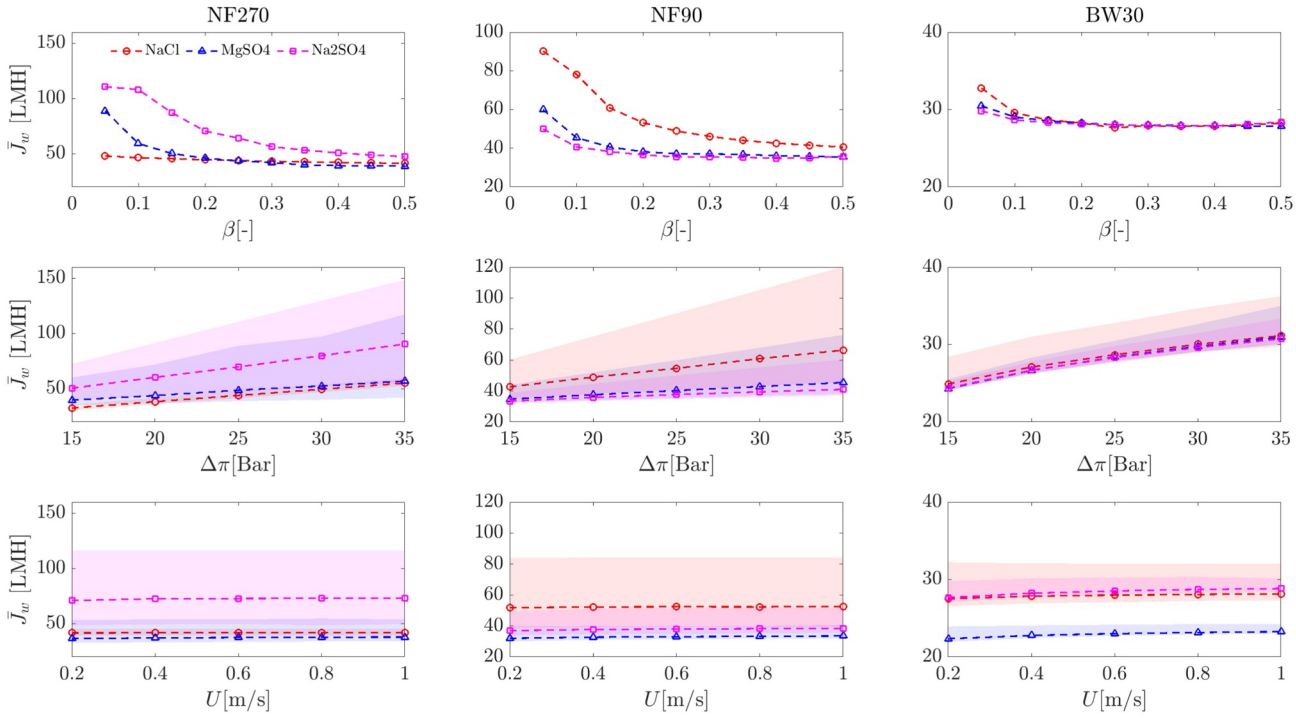

Fig. 5. Numerical solutions for the theoretical model using varying parameters and their effect on the mean water flux (spatially averaged along the membrane), $\bar{j}_w$ [LMH], temporally averaged over the OBW duration which was defined as the time it takes to reach $j_w = 5\mu$m/s $\approx$ 18LMH. The first, second and third rows shows the effect of the hindered support diffusivity β, the initial osmotic pressure across the membrane $\Delta\pi$ [bar], and the cross flow velocity U [m/s] in the feed side, respectively. The respectively colored shaded regions are the value ranges for different values of $\beta \in$ [0.05,0.5] and the solid lines are the mean.

importantly, the initial flux is higher. Finally, the model calculations show that the osmotic flux is insensitive to the crossflow velocity, U, within the range of parameters examined. This is because the flux decline is dominated by internal polarization within the membrane, which is not affected by the crossflow. Further, the time scale for establishing the external concentration polarization is very short, and so this initial flux decline does not contribute to the cycle-averaged osmotic flux.

A second set of calculations was made for similar scenarios, but showing the osmotic flux averaged over the entire backwash cycle (see Fig. 5). Here, the trend with β is inverted; however, this is not a true reduction of the osmotic flux, but merely a reflection of the prolonged backwash duration. Combinations of membrane/solute with good retention become insensitive to β at some point, as the main determinant of flux becomes the external mass transfer. In the case of increased osmotic draw solution concentration, the cycle-averaged osmotic permeation rate increases for all combinations considered. Notably, the sensitivity of the SO_4^{-2} salts to changes in β is more pronounced for the NF membranes due to the lower molecular diffusivity. Finally, model calculations show that, as explained above for the backwash duration, the cycle-averaged osmotic flux is insensitive to the external mass transfer, at the velocities examined (exceeding 0.2 m/s which is typical for RO operation). However, it should be noted that even if the effect of the crossflow rate on osmotic backwash duration is negligible, it may still affect cleaning efficiency due to the higher shear force exerted on the foulant layer.

4.3. Osmotic cleaning of NF membranes fouled by mineral scale

As a preliminary test of the osmotic backwash's ability to clean a fouled surface, a series of fouling and cleaning experiments were conducted, in which calcium phosphate was used as the foulant due to its relevance to wastewater reclamation at high recovery. Flux measurements from a representative experiment are shown in Fig. 6, in which the permeate flux, scaled against its initial value, is monitored until it declines by 50% due to scaling. Two cleaning protocols are shown - the first is a physical wash (PW) applied for 30 min, resulting in a low degree of flux restoration. Then, the flux was allowed to decline to 40% of its initial value, upon which a five-minute osmotic backwash was applied, restoring the flux to the same value as the 30-min physical wash. This serves as a small indication of the better cleaning potential achieved by the osmotic backwash, as it commences at a point where the membrane was more fouled, applied over a much shorter duration and achieved better flux restoration. This is further illustrated in a series of scanning electron microscopy images (see Fig 6) of the pristine, fouled and cleaned membrane - using the two methods. While this is far from showing the full potential, it is nonetheless indicative since both methods are 'physical' in nature - a chemical rinse at a low pH would be the normal way to remove scale, but this comes at a cost of membrane damage, providing the motivation to replace it with more benign methods.

As a further illustration, several similar experiments were conducted with varying application times of the two cleaning protocols. Furthermore, the initiation point of the cleaning protocols was also varied between extremely severe fouling (where the flux was reduced to $\sim$ 25% of its initial value) through to a lower degree of fouling (initiated at a flux of $\sim$ 75% of its initial value). This was done so as to gain some insight on the effect of timing on cleaning efficiency - one may envision this to be an indication of the cleaning frequency required for sustained operation. The results, presented in Fig. 7, show that cleaning effectiveness is affected by the duration of its application - performing a 5-min vs. 20-min OBW, commencing at similar fouling conditions, resulted in a flux restoration to $\sim$ 65% and $\sim$ 90% of the initial flux, respectively. A similar trend was observed for the PW, but the combination of an earlier fouling stage with an increase in duration provided a smaller contribution to the cleaning efficiency. Curiously, our earlier results showed that at times greater than 10 min, no

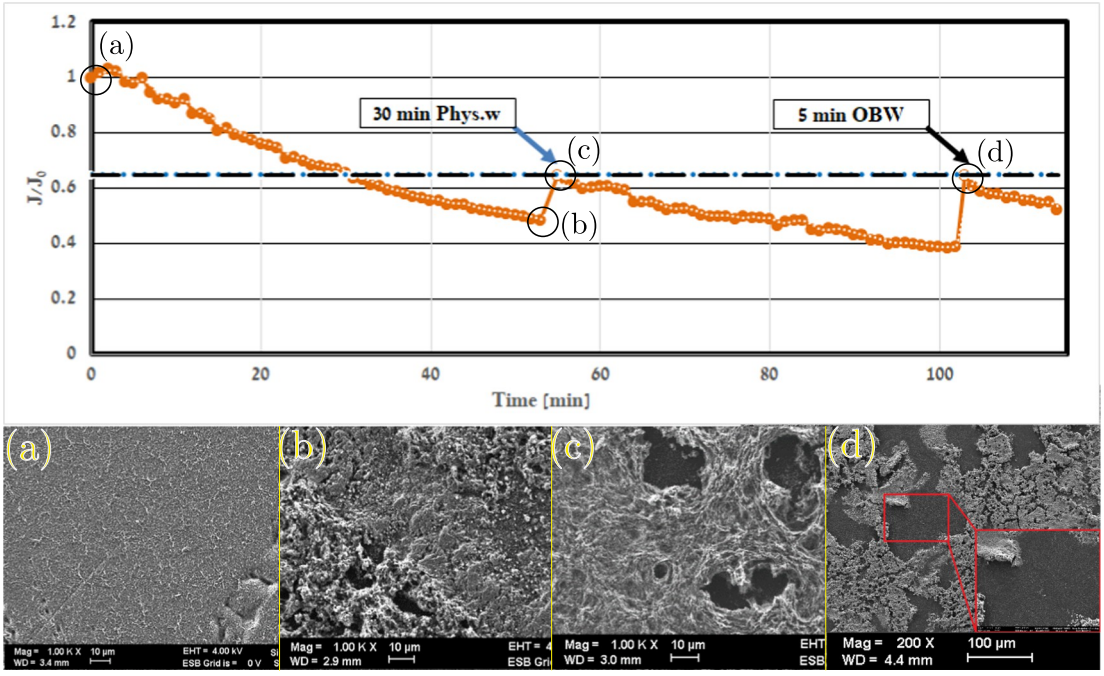

Fig. 6. Relative flux vs. time during a fouling experiment followed by a 30 min PW and a 5[min] OBW. The NF90 Membrane was taken after specific steps of the fouling and cleaning experiments for SEM imaging. (a) Clean membrane after compaction; (b) after a fouling cycle; (c) after 30 min PW; (d) after 5 min OBW.

significant backwash is actually present, meaning that the reminder of the OBW would be more akin to the PW and so a 20-min OBW may be considered as a combination of the two methods. It is possible that the osmotic backwash acts as a ' loosening' stage and the high shear applied concurrently eventually removes the looser scale, possibly breaking off pieces that were not strongly adhered to the membrane in the first place; similar results were seen during combined backwashing and physical cleaning of FO membranes [17]. Notably, a 5-min OBW applied when the fouling was less severe (represented by a flux decline to ~ 75% of its initial value) resulted in practically full flux restoration. However, this is not by any means conclusive evidence that a longer backwash is, in fact, better. For example, Jiang et al. [18] found that flux recovery saturated after 10 min, although this could also be due to loss of osmotic permeation after this period. Further optimization should be carried out before any conclusions may be made.

5. Concluding remarks

The results obtained in the reported study demonstrate that, while NaCl has been shown to be effective for seawater-RO, it is not quite the case for brackish-RO and NF membranes, where salt leakage through the membrane and the resulting internal concentration polarization within the support result in rapids decline of the backwash flux. Switching to sulphate-based draw solutions considerably improved the ability to sustain an osmotic backwash for longer times, even in the case of NF. Model calculations, shown to be in general good agreement with the experimental measurements, illustrate the sensitivity of the backwash flux on the hinderance to diffusion and the osmotic driving force (presented by the support structure). Finally, a set of experiments was conducted to provide preliminary indication of the cleaning potential of osmotic backwashing for removing scale precipitated on NF membranes. The tests showed that the backwash, as may be expected,

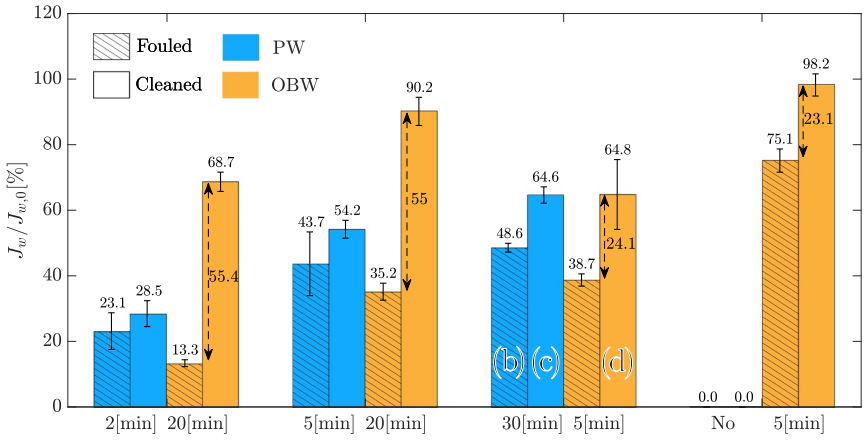

Fig. 7. The relative flux (respective to the flux at the pristine state) in four different sets of experiments comparing cycles of PW (i.e. only cross flow) and OBW, at different levels of fouling. The cleaning cycles were performed for 0, 2, 5 and 30 min long for PW; for 5 and 20 min long for OBW. In each experiment we present the mean flux per cent before (patterned) and after (solid) each treatment. The error bars are the respective standard deviations. The columns of the third experiment are each marked with a letter corresponding to a SEM image shown in Fig. 6, (a) which is not listed corresponds to a pristine membrane, i.e. 100% relative flux.

possibly adds a 'loosening' effect which, combined with the shear induced by the crossflow, removes the scale from the membrane surface. This is evident by the shorter duration required and superior cleaning efficiency achieved in the presence of the backwash, as compared with crossflow cleaning alone. Moreover, results show the importance of timing on backwash efficiency, whereupon the application of a 5-minute backwash after ~ 25% flux loss achieves nearly complete restoration, while backwashing after the flux reduced to ~ 20% and ~ 40% of its initial value restored it to ~ 60% and ~ 90%, for a 20-minute backwash. These results provide initial proof of the potential viability of osmotic backwashing as a cleaning protocol for membranes used for brackish- and waste-water desalination. Further work is required in order to optimize process conditions, e.g. the frequency, duration and intensity of the backwash.

Nomenclature

B	Membrane salt permeability $[\frac{m}{s}]$
c	Concentration $[\frac{mole}{m^3}]$
$\bar{c}$	Logarithmic mean concentration, $\frac{c_f - c_p}{\ln(c_f / c_p)} \frac{mole}{m^3}]$
D	Molecular diffusion coefficient $[\frac{m^2}{s}]$
k	Mass transfer coefficient $[\frac{m}{s}]$
j	Permeation rate $[\frac{m^3}{m^2 s}]$
δ	Feed channel length, $\frac{D_f}{k}$ [m]
L	Support channel length, $[m]$
L_p	Membrane permeability coefficient $[\frac{m^3}{m^2 s \cdot Pa}]$
Δp	Trans-membrane pressure [Pa]
i	Van't Hoff factor [-]
R_g	Universal gas constant $[\frac{J}{mole \cdot K}]$
t	Time $[s]$
T	Temperature $[K]$
v	Axial velocity component $[\frac{m}{s}]$
y	Axial coordinate $[m]$

Greek letters

β	Diffusion hinderance factor, [-]
ϵ	Porosity [-]
τ	Tortuosity [-]
σ	Reflection coefficient [-]
Φ	Osmotic coefficient [-]

Subscripts

b	Bulk
m	Membrane
f	Feed
p	Permeate

Abbreviations

ADE	Advection-diffusion equation
CP	Concentration polarization
RO	Reverse osmosis

Acknowledgments

This research was funded by the US-Israel Binational Agricultural R &D fund (BARD), grant number S-4768-14R.

References

[1] J. Vrouwenvelder, S. Bakker, M. Cauchard, R. Le Grand, M. Apacandié, M. Idrissi, S. Lagrave, L. Wessels, J. van Paassen, J. Kruithof, M. van Loosdrecht, The membrane fouling simulator: a suitable tool for prediction and characterisation of membrane fouling, Water Sci. Technol. 55 (8-9) (2007) 197–205.
[2] Y. Le Gouellec, Calcium sulfate (gypsum) scaling in nanofiltration of agricultural drainage water, J. Membr. Sci. 205 (1-2) (2002) 279–291.
[3] A. Antony, J.H. Low, S. Gray, A.E. Childress, P. Le-Clech, G. Leslie, Scale formation and control in high pressure membrane water treatment systems: a review, J. Membr. Sci. 383 (1-2) (2011) 1–16.
[4] C. Fritzmann, J. Löwenberg, T. Wintgens, T. Melin, State-of-the-art of reverse osmosis desalination, Desalination 216 (1-3) (2007) 1–76.
[5] M. Qasim, M. Badrelzaman, N.N. Darwish, N.A. Darwish, N. Hilal, Reverse osmosis desalination: a state-of-the-art review, Desalination 459 (2019) 59–104.
[6] K. Spiegler, J. Macleish, Molecular (osmotic and electro-osmotic) backwash of cellulose acetate hyperfiltration membranes, J. Membr. Sci. 8 (2) (1981) 173–192.
[7] A. Sagiv, R. Semiat, Backwash of RO spiral wound membranes, Desalination 179 (1-3) (2005) 1–9.
[8] J.-J. Qin, M.H. Oo, K.A. Kekre, B. Liberman, Development of novel backwash cleaning technique for reverse osmosis in reclamation of secondary effluent, J. Membr. Sci. 346 (1) (2010) 8–14.
[9] B. Liberman, Simultaneous power recovery of gauge and osmotic pressure from brine of SWRO desalination plants, Desalin. Water Treat. 15 (1-3) (2010) 249–255.
[10] A. Sagiv, N. Avraham, C.G. Dosoretz, R. Semiat, Osmotic backwash mechanism of reverse osmosis membranes, J. Membr. Sci. 322 (1) (2008) 225–233.
[11] G. Ramon, Y. Agnon, C. Dosoretz, Dynamics of an osmotic backwash cycle, J. Membr. Sci. 364 (1) (2010) 157–166.
[12] A. Sagiv, R. Semiat, Modeling of backwash cleaning methods for RO membranes, Desalination 261 (3) (2010) 338–346.
[13] G.Z. Ramon, T.-V. Nguyen, E.M. Hoek, Osmosis-assisted cleaning of organic-fouled seawater RO membranes, Chem. Eng. J. 218 (2013) 173–182.
[14] E. Bar-Zeev, M. Elimelech, Reverse osmosis biofilm dispersal by osmotic backflushing: cleaning via substratum perforation, Environ. Sci. Technol. Lett. 1 (2) (2014) 162–166.
[15] E. Bar-Zeev, F. Perreault, A.P. Straub, M. Elimelech, Impaired performance of pressure-retarded osmosis due to irreversible biofouling, Environ. Sci. Technol. 49 (21) (2015) 13050–13058.
[16] E.S.H. Lee, J.Y. Xiong, G. Han, C.F. Wan, Q.Y. Chong, T.-S. Chung, A pilot study on pressure retarded osmosis operation and effective cleaning strategies, Desalination 420 (2017) 273–282.
[17] J. Kim, G. Blandin, S. Phuntsho, A. Verliefde, P. Le-Clech, H. Shon, Practical considerations for operability of an 8 spiral wound forward osmosis module: hydrodynamics, fouling behaviour and cleaning strategy, Desalination 404 (2017) 249–258.
[18] W. Jiang, Y. Wei, X. Gao, C. Gao, Y. Wang, An innovative backwash cleaning technique for NF membrane in groundwater desalination: fouling reversibility and cleaning without chemical detergent, Desalination 359 (2015) 26–36.
[19] M. Mulder, Basic Principles of Membrane Technology, Second edition, (1997).
[20] N. Hilal, H. Al-Zoubi, A.W. Mohammad, N. Darwish, Nanofiltration of highly concentrated salt solutions up to seawater salinity, Desalination 184 (1-3) (2005) 315–326.
[21] H. Al-Zoubi, N. Hilal, N. Darwish, A.W. Mohammad, Rejection and modelling of sulphate and potassium salts by nanofiltration membranes: neural network and Spiegler-Kedem model, Desalination 206 (1-3) (2007) 42–60.
[22] Y. Boussouga, A. Lhassani, Study of mass transfer mechanisms for reverse osmosis and nanofiltration membranes intended for desalination, J. Mater. Environ. Sci. 8 (3) (2017) 1128–1138.
[23] M. Pontié, H. Dach, J. Leparc, M. Hafsi, A. Lhassani, Novel approach combining physico-chemical characterizations and mass transfer modelling of nanofiltration and low pressure reverse osmosis membranes for brackish water desalination intensification, Desalination 221 (1-3) (2008) 174–191.
[24] G.Z. Ramon, E.M. Hoek, On the enhanced drag force induced by permeation through a filtration membrane, J. Membr. Sci. 392-393 (2012) 1–8.